



HAL
open science

A new borrowing hydrogen mechanism for redox-active metals

Priyanka Chakraborty, Basker Sundararaju, Eric Manoury, Rinaldo Poli

► To cite this version:

Priyanka Chakraborty, Basker Sundararaju, Eric Manoury, Rinaldo Poli. A new borrowing hydrogen mechanism for redox-active metals. *ACS Catalysis*, 2021, 11, pp.11906-11920. 10.1021/acscatal.1c02616 . hal-03244195v1

HAL Id: hal-03244195

<https://hal.science/hal-03244195v1>

Submitted on 3 Jun 2021 (v1), last revised 29 Sep 2021 (v2)

HAL is a multi-disciplinary open access archive for the deposit and dissemination of scientific research documents, whether they are published or not. The documents may come from teaching and research institutions in France or abroad, or from public or private research centers.

L'archive ouverte pluridisciplinaire **HAL**, est destinée au dépôt et à la diffusion de documents scientifiques de niveau recherche, publiés ou non, émanant des établissements d'enseignement et de recherche français ou étrangers, des laboratoires publics ou privés.

Article

A new borrowing hydrogen mechanism for redox-active metals

Priyanka Chakraborty,¹ Basker Sundararaju,^{1,*} Eric Manoury,² and Rinaldo Poli^{2,3,4,**}¹Department of Chemistry, Indian Institute of Technology Kanpur, Kanpur, Uttar Pradesh 208016, India²CNRS, LCC (Laboratoire de Chimie de Coordination), Université de Toulouse, UPS, INPT, 205 Route de Narbonne, BP 44099, F-31077, Toulouse Cedex 4, France³Institut Universitaire de France, 1, rue Descartes, 75231 Paris Cedex 05, France⁴Lead contact*Correspondence: basker@iitk.ac.in**Correspondence: rinaldo.poli@lcc-toulouse.fr

SUMMARY

Three different but mechanistically related Cp*Co^{III}/base-catalyzed “borrowing hydrogen” alkylations by secondary alcohols with C-N or C-C bond formation have been scrutinized by DFT calculations and experiments. They all follow a new paradigm, whereby the metal-coordinated alkoxide is oxidized to ketone by transfer of the β-H as a proton to an internal or external base (and two electrons to the metal), rather than as a hydride via the ubiquitous β-H elimination. Stoichiometric experiments show the formation of unusual species, including the 20-electron spin triplet carbonyl complex, [Cp*Co(quinOH)(CO)] (quinOH = 8-hydroxyquinoline). DFT calculations reproduced the observed relative stabilities and the ground states of all molecules and suggest ligand non-innocence for certain intermediates. They also pinpoint the key rate-determining steps of the catalytic cycles, yielding cycle span parameters in agreement with the experiment, and rationalize the observed selectivities.

Keywords: Borrowing Hydrogen; Cobalt; DFT Calculations; Hydrogen transfer; Paramagnetic organometallics

Dedicated to Christian Bruneau for his outstanding contribution to catalysis

INTRODUCTION

Hydrogenations undoubtedly occupy a dominant role in the area of transition metal homogeneous catalysis in terms of both fundamental investigations and applications.^{1–8} The processes of transferring two H atoms to a substrate and its reverse (dehydrogenation)^{9,10} are also involved in a host of other catalyzed transformations such as hydroformylation and transfer hydrogenation, as well as in a growing family of reactions that take place through the “hydrogen-borrowing” strategy¹¹ such as olefin hydroaminomethylation,¹² alkane metathesis,¹³ carbonyl reductive coupling,¹⁴ etc. The catalyzed transfer of two H atoms to/from a substrate has a very rich mechanistic landscape. All highlighted pathways to date can be grouped into two fundamental families, both including several variants. In the first one (Scheme 1a), both H atoms transit through the catalytic metal center as hydride ligands and two electrons are provided by the metal ion, which shuttles through the Mⁿ/Mⁿ⁺² formal oxidation states. The transformation may occur via a monohydride (a1) or a dihydride (a2) cycle and the substrate functionalization, typically occurring by coordination/insertion, may occur either before or after the H₂ activation step.¹ However, the two H atoms in the Mⁿ⁺²(H)₂ intermediate may also be transferred to an outer sphere unsaturated substrate as H⁺ and H⁻ (a3).¹⁵ Mechanisms that allow the Y/YH₂ interconversion without the incorporation/release

The bigger picture

The present investigation has unveiled a new mechanistic paradigm for transfer hydrogenation and borrowing hydrogen processes, which are involved in a growing number of efficient chemical transformations making use of readily available alcohols as alkylating agents and generating only water as waste product. They are consequently greener processes, bypassing more traditional methods to achieve the same transformation, which make use of toxic reagents and produce more waste.

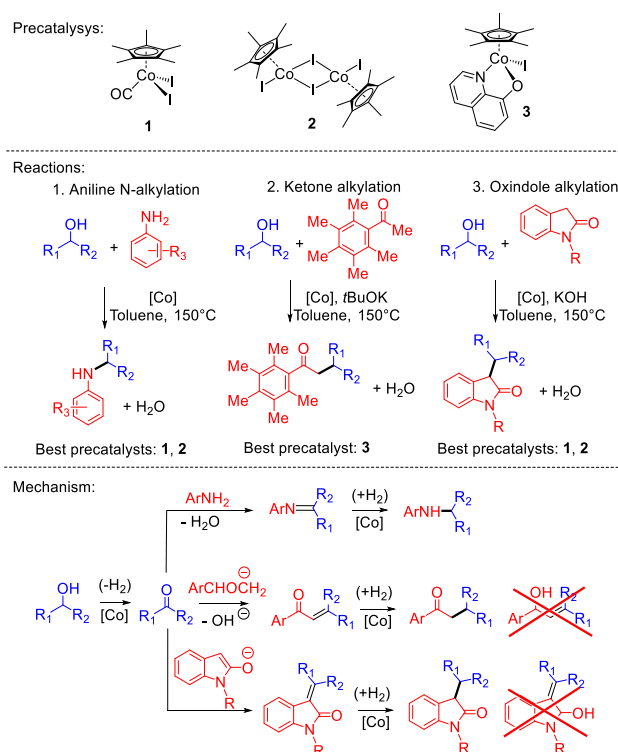
We show the first example of a dehydrogenative activation of the alcohol substrate by transfer of the C-bonded H atom as a proton to an internal or external base, with the catalytic metal acting as an electron repository. This process is promoted by a Cp*Co^{III}-based catalyst. This new mechanistic understanding can inspire the development of better catalysts for this important family of transformations.

be followed). A reversible mode for the second step in catalyzed hydrogen transfer processes has not been previously highlighted to the best of our knowledge. The details of this study, which also allows to rationalize the observed selectivity, are described in the present contribution.

RESULTS AND DISCUSSION

(a) Best catalyst - reaction combinations

In our recent work, the three different Cp*Co^{III} precatalysts **1-3** (Scheme 2) were tested in three different but mechanistically similar reactions, all involving a secondary alcohol as alkylating agent and a substituted aniline,²⁷ an alkyl pentamethylphenyl ketone,²⁸ or an oxindole²⁹ as substrate, respectively, resulting in C-N bond formation for the first reaction and C-C bond formation for the second and third ones. Experimental mechanistic studies have demonstrated the occurrence of a hydrogen-borrowing mechanism in all cases, as detailed in Scheme 2, with the metal complex facilitating the dehydrogenation/hydrogenation steps, whereas the C-N and C-C bond formations occur without participation of the metal complex.

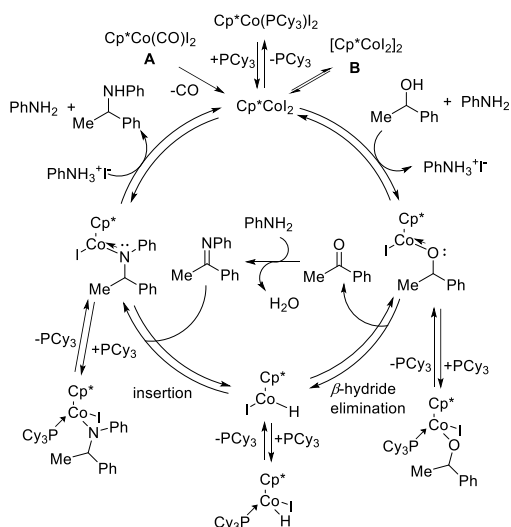


Scheme 2. Precatalysts, reactions, and hydrogen-borrowing mechanisms

Reactions that follow the same initial secondary alcohol dehydrogenation in the borrowing hydrogen path and precatalysts (**1-3**) with different relative performance for the different reactions.

For the oxindole alkylation reactions, **1** and **2** perform equally well and better than **3**,²⁹ justifying the proposition that both lead to a common unsaturated [Cp*CoL₂] species by either CO dissociation or bridge splitting. For the aniline alkylation reaction, **1** was also shown to be active and the activity was improved by the presence of a bulky phosphine additive (PCy₃).²⁷ A rationalization of the alcohol dehydrogenation mechanism, as proposed in the aniline alkylation study²⁷ and recalled in Scheme 3, appeared rather straightforward: the alcohol molecule is reduced by a sequence of equilibrium deprotonation, coordination (by substitution of an iodide ligand) and β-H elimination, to afford a hydride intermediate [Cp*CoH]. The imine resulting from the uncatalysed ketone-amine condensation is then reduced through the reverse steps. This mechanism is a variant of pathway b1 in Scheme 1 where the proton is delivered by the ammonium ion rather than by H₂. DFT calculations on

the key cycle intermediate suggested the feasibility of all steps from the thermodynamic point of view, but no transition states were explicitly located.²⁷ The calculations also suggested that PCy₃ reversibly coordinates to the unsaturated intermediates, particularly to the hydride complex, stabilizing them and perhaps protecting them from unwanted catalyst degradation pathways.



Scheme 3. Possible pathway for aniline alkylation by hydrogen borrowing

Catalytic cycle proposed in a previous contribution²⁷ for the aniline hydrogen borrowing alkylation.

For the oxindole alkylation, a similar cycle can be imagined, although there is an important difference in terms of the base strength (*t*BuOK instead of PhNH₂) and a selectivity issue in the final hydrogenation step. We will return to these issues in a later section. For the ketone alkylation reaction, on the other hand, catalyst **3** was found to outperform **1** and **2**, even when the latter precatalysts were used in the presence of PCy₃.²⁸ On the basis of the mechanism shown in Scheme 3, it is unclear how **3** could be a better catalyst because, after exchange of the single iodide ligand with alkoxide, no open coordination site remains available on the metal center to receive the hydride ligand, unless the oxyquinoline partially decoordinates or the Cp* ring slips from η⁵ to η³ or η¹. Another issue is the selectivity of the ketone alkylation reaction, since the last step of the reaction (hydrogenation of the α,β-unsaturated ketone produced by the condensation process) could potentially occur either at the C=C or C=O bond, but only the former was observed. Therefore, additional investigations were carried out. Before detailing the investigations on system **3**, which revealed the existence of an unsuspected new pathway, we describe more detailed calculations on the β-H elimination pathway for alcohol dehydrogenation by the [Cp*Co]₂/PhNH₂ system (Scheme 3), including the location of the transition states, even if this pathway will ultimately turn out not to be the preferred one. Besides revealing interesting features for half-sandwich Co^{III} compounds with hard donor ligands, these results will serve as a useful reference for the subsequent sections.

(b) Probing alcohol dehydrogenation by β-H elimination with [CpCo]₂/PhNH₂

The previously published DFT investigation²⁷ only considered singlet states. However, the high electron pairing energies experienced by the valence electrons of first-row metals in relatively high oxidation states may favor higher spin states.³² Indeed, the additional calculations indicate that all open-shell species involved in the Scheme 3 cycle are more stable with a triplet state configuration. These calculations were carried out at the same level of theory as the previous ones, namely using the dispersion-corrected B₃LYP-D₃ functional (see Computational Details), 2-phenylethanol as model alcohol, aniline as base, and the unsubstituted Cp ring as a simpler model of the Cp* ligand to reduce the computational cost. The reaction was nevertheless explored also along the singlet state potential energy surface and the results are summarized in Figure 1.

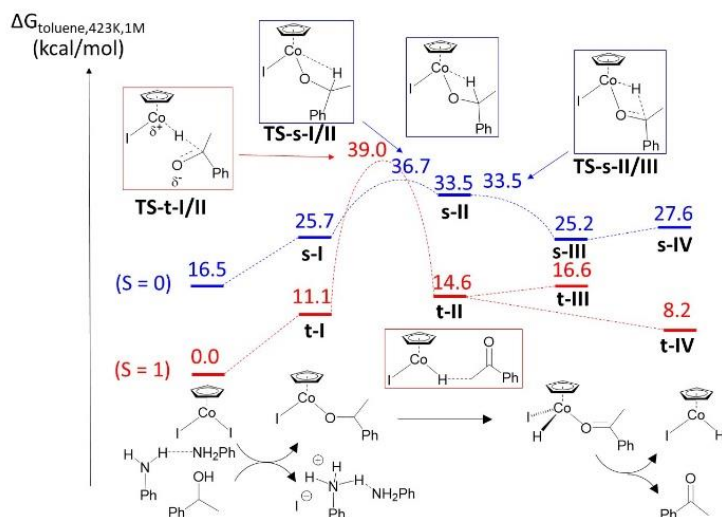


Figure 1. Alcohol β -H transfer to cobalt.

B_3LYP -calculated free energy profile at 150°C in toluene for the transformation of 2-phenylethanol, $[Cp^*CoI_2]$ and $PhNH_2 \cdots PhNH_2$ to acetophenone, $[CpCoIH]$ and $PhNH_2 \cdots PhNH_3^+I^-$.

For the starting $[CpCoI_2]$ complex, the free energy of the singlet state is 16.5 kcal/mol higher than that of the triplet state at 150°C in toluene. Replacement of one iodide ligand with the 2-phenylethoxide leads to complex $[CpCo(OCHMePh)]$ (I), which was found again more stable in the triplet state (t-I), with the singlet s-I isomer placed 14.6 kcal mol⁻¹ higher. This ligand exchange costs 16.2 kcal mol⁻¹ on the ΔG scale at 150°C (12.2 kcal mol⁻¹ at 298 K) when the 2-phenylethanol substrate is deprotonated by an aniline molecule to yield $PhNH_3^+I^-$. However, a better model for the protonated aniline is the homoconjugate acid-base adduct, $[PhNH_3 \cdots H_2NPh]^+I^-$. This interaction provides an additional ΔG stabilization of 5.1 kcal mol⁻¹ at 150°C to the system, so that t-I is now located at only 11.1 kcal mol⁻¹ from the starting $[CpCoI_2] + PhNH_2 \cdots H_2NPh$ system. A possible second iodide substitution has also been considered, leading to a hypothetical bis(alkoxo) $CpCo^{III}$ intermediate. However, the cost of this second step (a methanol molecule was used as “spectator” alcohol for the sake of computational cost) brings the system to much higher free energy (28.8 kcal mol⁻¹ when using two $PhNH_2 \cdots H_2NPh$ to yield two $[PhNH_3 \cdots H_2NPh]^+I^-$), see details in the SI (section S1). This intermediate is therefore not further considered as a precursor leading to β -H elimination, for the present catalytic system. However, the energy profile will change in the presence of a stronger base (*vide infra*).

The intermediate I can potentially lead to $[Cp^*CoIH]$ and acetophenone via a β -H elimination mechanism. Indeed, this can occur in two steps along the singlet surface via an effectively saturated agostic intermediate s-II where the alkoxide β -C-H bond interacts with the open coordination site of the cobalt complex, before the final C-H bond breaking step. The first transition state (TS-s-I/II) has the highest relative G value (36.7 kcal/mol from spin triplet $[CpCoI_2]$), yielding s-II at 33.5 kcal mol⁻¹. The latter proceeds via a very small barrier through transition state TS-s-II/III to produce the singlet acetone complex, $[CpCoIH(O=CMePh)]$ (s-III), located at 25.2 kcal mol⁻¹. Acetophenone dissociation to generate the singlet 16-electron $[CpCoIH]$ product (s-IV) has only a small ΔG cost. However, the latter complex was once again found more stable in the triplet state (t-IV). The triplet-singlet gap is ca. 20 kcal mol⁻¹, locating the t-IV product (plus acetophenone and $[PhNH_3 \cdots H_2NPh]^+I^-$) at 8.2 kcal mol⁻¹ from the reagents. It is of interest to note that even the 18-electron acetophenone adduct prefers a triplet configuration (t-III), although the differential is smaller than for the less saturated compounds. The preference of a triplet state for electronically saturated organometallic complexes has precedents,³² a notable example being the acetone complex $[Cp^*Fe(dppe)(Me_2CO)]^+$.³³ This preference results from a rather loose ketone coordination in the triplet complex (Co-O distance of 2.247 Å, vs. 1.977 Å in the singlet adduct), which is insufficient to raise the energy of the antibonding orbital to the point where electron pairing

would occur. Complex **t-III**, however, although yielding a stable local minimum, has a higher free energy than the **t-IV**...acetophenone van der Waals adduct (**t-II**), which features a hydride-methyl interaction as the shortest contact ($H\cdots H = 2.48 \text{ \AA}$).

The acetophenone generation along the triplet potential energy surface (PES), on the other hand, does not occur via a β -H elimination mechanism, which would require placing one electron in a high energy antibonding orbital for the agostic intermediate. All attempts to optimize the structure of this putative triplet intermediate led back to the starting 16-electron alkoxide complex. Through a series of relaxed scans (all the details are in the supporting information, section S2), the operating mechanism was identified as a Co-O bond breaking leading to a transition state **TS-t-I/II** that may be describe as a σ -complex of the $CpCo^+$ cation with the β -C-H bond of the $PhCH(Me)O^-$ anion, $\{CpCo^+\cdots H-C(Me)(Ph)O^-\}$, then proceeding to Co-H strengthening and C-H weakening with direct formation of the van der Waals adduct **t-II**. The free energy of this rate-determining transition state is calculated as $39.0 \text{ kcal mol}^{-1}$ relative to the reagents. The same mechanism was also reported for the dehydrogenation of isopropanol to acetone on a diamagnetic (*p*-cymene) Ru^{II} system supported by a chelating iminophosphonamide ligand.³⁴ In that case, the β -H elimination pathway is blocked by the strong chelating power of the NPN ligand in the electronically saturated $[(p\text{-cymene})Ru(ArNPPH_2NAR)(OiPr)]$ intermediate ($Ar = p\text{-tolyl}$), whereas the pathway via the $\{(p\text{-cymene})(ArNPPH_2NAR)Ru^+\cdots H-CMe_2O^-\}$ is stabilized by strong H-bonding interactions between the alkoxide and the alcohol solvent molecules. It is quite likely that an H-bonding assistance also occurs for the present system, significantly lowering the ketone elimination barrier. This barrier would then most probably become lower than the highest point on the singlet surface, avoiding the presence of spin crossover. Calculations on a more realistic model, however, were not carried out, because an alternative and lower-energy pathway (detailed further down) was discovered in the meantime. The observed activity (e.g. yield of 81% in 24 h with a 10% catalyst loading for the alkylation of *p*-anisidine with 2-phenylethanol²⁷) yields a lower estimate of 0.34 h^{-1} for the turnover frequency (TOF), for which the energy span upper limit is 33 kcal/mol according to the Eyring relationship.

We have also given some consideration to the possible bias that the chosen hybrid B₃LYP functional may introduce in favor of the higher spin state.³⁵ In order to estimate the extent of this bias, all singlet-triplet gaps were also obtained after geometries reoptimization with the BPW₉₁* functional (see Computational Details), for which excellent results against experimental benchmarks were previously obtained in other investigations of first-row transition metal chemistry (Fe, Co).^{36,37} Indeed, the gaps are slightly reduced as shown in **Erreur ! Source du renvoi introuvable.**, but not sufficiently to alter our conclusion that this ideal reaction pathway would prefer alkoxide dissociation followed by β -H transfer along the triplet PES. The energy profile of Figure 1 serves as a useful reference for the investigation of the model of catalyst **3**, which is described below. We will come back to the alcohol dehydrogenation step by $[Cp^*Co_2]/PhNH_2$ in a later section.

Table 1. Comparison of calculated triplet-singlet gaps

Molecule	B ₃ LYP-D ₃	BPW ₉₁ *-D ₃
[CpCo ₂]	16.5	14.8
I	15.1	13.0
III	6.7	3.3
IV	19.4	16.0

$[G(\text{singlet})-G(\text{triplet})]$ in toluene at 423K (1 M standard state) in kcal mol^{-1} for various molecules at the B₃LYP-D₃ and BPW₉₁*-D₃ levels

(c) Alcohol dehydrogenation with the $[CpCo(Oquin)]/tBuOK$ system

Given the greater size (higher number of electrons) relative to $[Cp^*Co_2]$, the calculations on this system used the smaller isopropanol molecule in addition to the simplification of the Cp^* ligand. This is a pertinent simplification because the ketone alkylation reaction (Scheme 2, reaction 2) also works quite well with aliphatic alcohols such as 2-heptanol, cyclopentanol or cyclohexanol, in addition to the preferred benzylic alcohols.²⁸ The 8-oxoquinolinato ligand (henceforth abbreviated as Oquin) was not simplified. Thus, the computational model for the

precatalyst **3** (Scheme 2) is CpCo(Oquin), **V**. All calculations were once again carried out with the B₃LYP-D₃ functional. The ketone alkylation reaction features one important difference relative to the amine alkylation: the alcohol deprotonation involves a stronger base (*t*BuOK). With this base, both the alcohol deprotonation and the iodide for alkoxide ligand exchange in **V** are spontaneous processes (SI, section S3). Therefore, complex [CpCo(Oquin)(OCHMe₂)] (**VI**) can be taken as the starting point of the catalytic cycle. The precatalyst **3** has been fully characterized, including by an X-ray structural analysis, as a diamagnetic compound.²⁶ In agreement with the experimental evidence, the calculations on the model system indeed indicate a slight preference for the singlet state **s-V** (singlet-triplet gap of 0.3 kcal/mol for *E* and 0.2 kcal/mol for *G* with solvent correction in toluene at 25°C). The comparison of the optimized structure with that determined by X-ray diffraction is also excellent (see SI, section S4). The 18-electron isopropoxide complex, on the other hand, yields a more stable triplet, **t-VI**, the singlet **s-VI** being less stable by 5.0 (*E*), 6.0 (*G*_{toluene,298K}) and 6.8 (*G*_{toluene,423K}) kcal mol⁻¹. Thus, the replacement of the harder O donor with the softer I has an important consequence on electron pairing, leading to a diamagnetic ground state. A reoptimization of **t-VI** and **s-VI** with the BPW91*-D₃ functional still yielded a more stable triplet state ($\Delta G_{\text{toluene},423\text{K}} = 6.0$ kcal/mol). The preferred high spin state for this 18-electron Co^{III} complex can be rationalized in the same way discussed above for the isoelectronic complex **III**.

From intermediate **VI**, whatever the spin state, the β -H elimination pathway leading to acetone and the cobalt(III) hydride complex [CpCo(Oquin)H] (**VII**) is not viable, unless an open coordination site is made available by partial Oquin dissociation, or by Cp ring slippage, or by ionic dissociation. All these pathways were explored (see details in the SI, sections S5 and S6) but found energetically too costly, although the reaction is thermodynamically exoergic: the calculated free energy for the combination of **s-VII** and acetone is located at -3.0 kcal mol⁻¹ relative to **t-VI**. The corresponding **t-VII** is only marginally higher (singlet-triplet gap = 1.1 kcal mol⁻¹). On the other hand, the various exploratory calculations led us to discover a new low-energy pathway. Firstly, we wondered whether a tautomeric [CpCo(quinOH)] complex (**VIII**), formally of cobalt(I), would be energetically accessible and what its ground state would be. The calculations indicated, somewhat unexpectedly, that this two-legged piano stool species is actually more stable than the three-legged piano stool hydride isomer when calculated as a spin triplet, **t-VIII**. The corresponding singlet state **s-VIII** is significantly less stable (Figure 2). The geometries of both **VII** and **VIII** tautomers are quite similar in the two spin states, except for the anticipated longer metal-ligand distances in the triplets. For **VIII**, the quinOH hydroxyl H atom is essentially coplanar with the CoNC₂O chelate ring (the O-H bond forms an angle with respect to the Oquin plane of ca. 22° for the singlet and essentially zero for the triplet). A literature search has not revealed any previous example of paramagnetic 18-electron half-sandwich cobalt(I) complexes, although this spin state has been observed for certain 16-electron systems such as tris-pyrazolylborato derivatives.^{38,39}

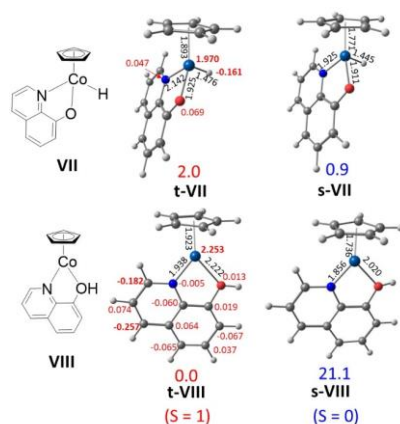


Figure 2. Geometry-optimized VII and VIII complexes

Views of the B₃LYP-D₃-optimized geometries and relative energies (in kcal mol⁻¹) of isomeric [CpCo(Oquin)H], **VII**, and [CpCo(quinOH)], **VIII**, in the singlet and triplet states. Selected bond distances (in Å) are shown in black characters and Mulliken spin densities in red characters.

The triplet ground state of **VIII** can be rationalized in the same way as for the above described 18-electron Co^{III} complexes **III** and **VI**: the low ligand field strength is unable to push the metal-ligand antibonding orbitals sufficiently high to induce spin pairing.³² A closer analysis of the **t-VIII** electronic structure, however, reveals a slightly more complicated situation: the calculated Mulliken spin density on the Co atom is greater than two electrons (2.253) and is compensated by negative spin density on the quinOH ligand, the highest values being on the quinoline 2-C (-0.182) and 4-C (-0.257) atoms. Thus, the compound is best described as the antiferromagnetic ($3/2, -1/2$) combination of a Co^{II} center and a hydroxyquinolinyl anion radical. The triplet hydride complex (**t-VII**), on the other hand, has the two unpaired electrons essentially localized on the Co atom (1.970), with the most significant remainder of the spin density on the Quin N and O atoms and a small negative contribution on the hydride.

Once realized that the quinOH cobalt complex **VIII** is relatively stabilized, we wondered whether a low-energy pathway exists for direct transfer of the alkoxide β -H atom to the ligand O atom. Indeed, this was calculated as an elementary step via a transition state located at only 14.5 kcal/mol from the triplet alkoxide complex **t-VI**, leading to a triplet [$\text{CpCo}(\text{quinOH})(\text{O}=\text{CMe}_2)$], **t-IX**, see Figure 3. The latter, although being formally a 20-electron compound, gave a stable local minimum along the triplet PES. Its electronic structure, like the one analyzed above for **t-VIII**, is of interest and will be further discussed in the next section. The acetone product dissociation leading to **t-VIII** is an exoergic process by 16.5 kcal mol⁻¹. The corresponding singlet system **s-IX** also yields a local minimum, located 5.4 kcal mol⁻¹ higher than the triplet, but this corresponds to an outer-sphere acetone adduct with a [$\text{CpCo}(\text{quinOH}\cdots\text{O}=\text{CMe}_2)$] interaction. The transition state **TS-t-VI/IX** has an imaginary frequency of 1012i cm⁻¹ and nearly equivalent H \cdots O (1.271) and H \cdots C (1.346 Å) distances. The calculated natural charges for the transferred H atom are 0.162 in **t-VI**, 0.372 in the transition state, 0.488 in **t-IX** and 0.494 in **t-VIII**, highlighting the increase of protic nature after the transfer. For comparison, the hydride atom has a natural charge of 0.144 in **s-VII** and 0.090 in **t-VII**. The natural charge of the cobalt atom shows smaller variations along the pathway of Figure 3 (respectively 0.762, 0.895, 0.850 and 0.693). Note that the same pathway has a much greater barrier along the singlet PES, as suggested by a relaxed scan on the O \cdots H distance (see SI, section S7).

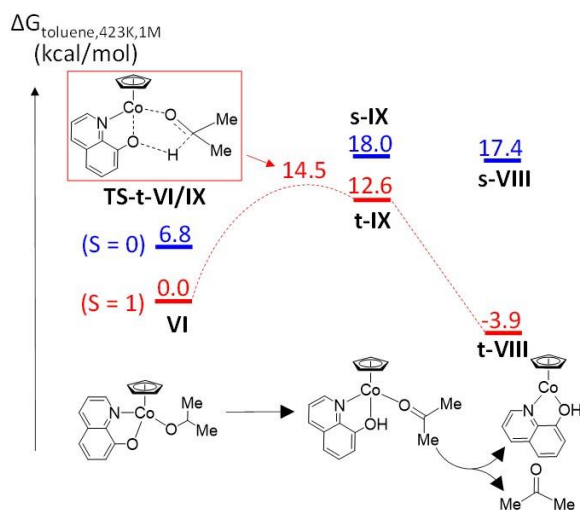


Figure 3. Conversion of VI to IX

$\text{B}_3\text{LYP-D}_3$ calculated free energy profile at 150°C in toluene for the transformation of [$\text{CpCo}(\text{Oquin})(\text{OCHMe}_2)$], **VI**, to acetone and [$\text{CpCo}(\text{quinOH})$], **IX**.

According to the DFT study, the unusual paramagnetic 18-electron system **t-VIII** may actually represent the resting state of the catalytic cycle because, in combination with the acetone coproduct, it is located at a lower free energy than the alkoxide precursor at 150°C. Under the standard conditions (25°C), on the other hand, the **t-VIII**/ Me_2CO combination has

a slightly greater **G** than **t-VI** (2.1 kcal mol⁻¹). This result has motivated new experiments aimed at generating and identifying this molecule, as described in the next section.

(d) Experimental investigations on Cp*Co(Oquin)-alkoxide systems

Treatment of **3** in toluene with isopropanol (1 equiv) and KOtBu (1 equiv) or with NaOiPr (1 equiv) at room temperature resulted in a color change (green to brown). The ¹H NMR analysis of the resulting solution in CDCl₃ indicated complete disappearance of the reactant resonances, but no new signal to replace them, indicating the paramagnetic nature of the brown product. The ¹H NMR spectrum could not confirm the presence of acetone in the crude mixture. This resonance is probably broadened by the reversible coordination to the paramagnetic cobalt center. Similar observations were made for the equivalent reactions between **3**/KOtBu and other secondary alcohols, generating brown solutions with a silent NMR spectrum and similar UV-visible spectra (see SI, section S8). To confirm the ketone formation, the corresponding KOCHPh₂ was separately prepared according to the literature procedure.⁴⁰ Reaction with **3** in toluene at 150 °C yielded again an NMR silent brown solution, from which benzophenone was isolated in a 70% yield, whereas the blank reaction run without the addition of **3** showed no ketone formation.

The same reaction with hexafluoroisopropanol (HFIP) at room temperature, on the other hand, resulted in the formation of yellowish-green, diamagnetic and thermally sensitive [Cp*Co(Oquin){OCH(CF₃)₂}]₂, **4**. No reaction occurred in the absence of KOtBu. The product could not be isolated in a pure form because of its thermal decomposition, which begun prior to the full conversion of **3** to **4**. When the **3**/HFIP/KOtBu reaction was carried out at higher temperatures, the color rapidly became brown and no NMR resonances could be observed for the final product. The identity of intermediate **4** was confirmed by an NMR investigation in CDCl₃ of the reaction mixture after incomplete consumption of **3**, prior to significant thermal decomposition. The ¹H NMR spectrum (see SI, section S8) shows upfield-shifted Oquin resonances, a new Cp* resonance at 1.2 ppm, and a septet at 1.8 ppm (³J_{HF} = 7.1 Hz) for the hexafluoroisopropoxide CH resonance, with quite different chemical shift and coupling parameters relative to free HFIP (δ 4.40 ppm, ³J_{HF} = 5.4 Hz). Integration of the Cp* resonances yielded a 4/3 ratio of ca. 2. The ¹⁹F NMR spectrum (Figure 4) shows two distinct resonances for the two CF₃ groups, which are rendered inequivalent by the Oquin ligand asymmetry and consequent central chirality at the metal atom, yielding two quartets in the ¹⁹F{¹H} spectrum and two doublets of quartets in the proton-coupled ¹⁹F spectrum with ⁴J_{FF} = 10.0 Hz and ³J_{FH} = 6.9 Hz for the δ -75.85 resonance and 7.4 Hz for the δ -76.29 resonance. The starred resonance centered at -75.2 ppm in Figure 4 is due to residual HFIP, presumably broadened by the H-bond equilibrium in **4**·HFIP. Additionally, small resonances with an equivalent pattern are visible slightly upfield from the two main resonances and may be attributed to a minor rotamer due to the restricted rotation of the hexafluoroisopropoxide group around the bulky Cp* ligand.

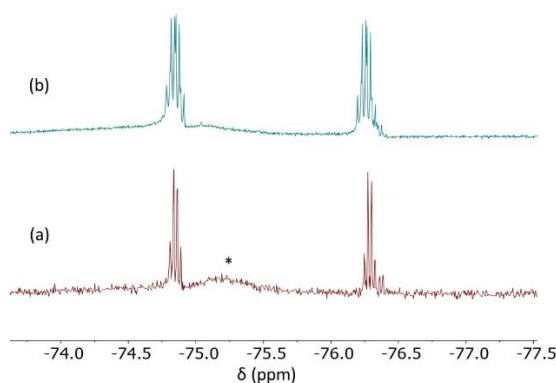


Figure 4. Characterization of 4.

¹⁹F{¹H} NMR (a) and ¹⁹F NMR (b) spectra of **4** in CDCl₃.

The experimental evidence of this alkoxide derivative, which is kinetically more stable and in a different spin state than the putative intermediate obtained from non-fluorinated alkoxides, provided an additional opportunity to benchmark the computational method. The Cp model system $[\text{CpCo}(\text{Oquin})\{\text{OCH}(\text{CF}_3)_2\}]$ (**t-VI^F**) was first calculated at the standard B₃LYP-D₃ level, yielding a ground state singlet, in agreement with the observed diamagnetism of compound **4**, although the triplet state is located only 1.2 kcal mol⁻¹ higher on the *E* scale. After the thermal corrections (*G*₂₉₈ scale), on the other hand, the triplet state is slightly preferred by 1.1 kcal mol⁻¹. Repeating the optimization at the B₃PWG₉₁-D₃ level gave a singlet ground state both on the *E* (by 3.2 kcal mol⁻¹) and *G*₂₉₈ (by 1.7 kcal mol⁻¹) scales. Therefore, the effect of the CHMe₂/CH(CF₃)₂ substitution on the stabilization of the singlet state is reproduced by the DFT calculations. It is interesting to observe that the alkoxide exchange in $[\text{Cp}^*\text{Co}(\text{Oquin})(\text{OR})]$ by two very different anionic ligands, I and OCH(CF₃)₂, has the same effect of favoring electron pairing. A possible reason of this effect may be the removal of the stronger π-donating alkoxide ligand (the O atom π-donor power in the hexafluoroisopropoxide ligand is expected to be significantly reduced by the electron-withdrawing CF₃ groups).

The calculations also reproduce the experimental stability trend. The β-H transfer from the OCH(CF₃)₂ ligand to the Oquin ligand to afford $[\text{CpCo}(\text{quinOH})\{\text{O}=\text{C}(\text{CF}_3)_2\}]$ (**t-IX^F**) through the transition state **TS-t-VI^F/IX^F** has a greater barrier than the corresponding β-H transfer from the OiPr ligand (19.5 vs. 14.9 kcal mol⁻¹ at 298 K), see Figure 5. The decomposition of **4** probably does not lead to the same paramagnetic species obtained from **3** (i.e. the Cp* equivalent of **t-VIII**) because the dissociation of (CF₃)₂CO from **t-IX^F** is predicted as highly endoergic. Rather, according to the computational investigation, a Co^{III} enolate appears easily accessible by HF elimination (see SI, section S8). Note how the Oquin OH proton in the optimized **t-IX^F** structure establishes a stabilizing F...H interaction involving one of the CF₃ groups (1.804 Å), whereas the corresponding optimized **t-IX** structure features a C...H interaction with the acetone carbonyl function (1.992 Å), from which it originated in the β-H transfer process. These interactions induce a significant deviation of the O-H bond from the Oquin plane (by ca. 66° in **t-IX** and 41° in **t-IX^F**), whereas the O-H bond is essentially coplanar with the Oquin ring in the ketone-free **VIII** as pointed out above. In addition, the carbonyl C atom in **t-IX** is still significantly pyramidalized (sum of the CCC and two OCC angles = 354.0°), attesting to the presence of a residual C...H interaction, whereas the same atom has a trigonal planar geometry (sum of the three angles = 159.9°) in **t-IX^F**.

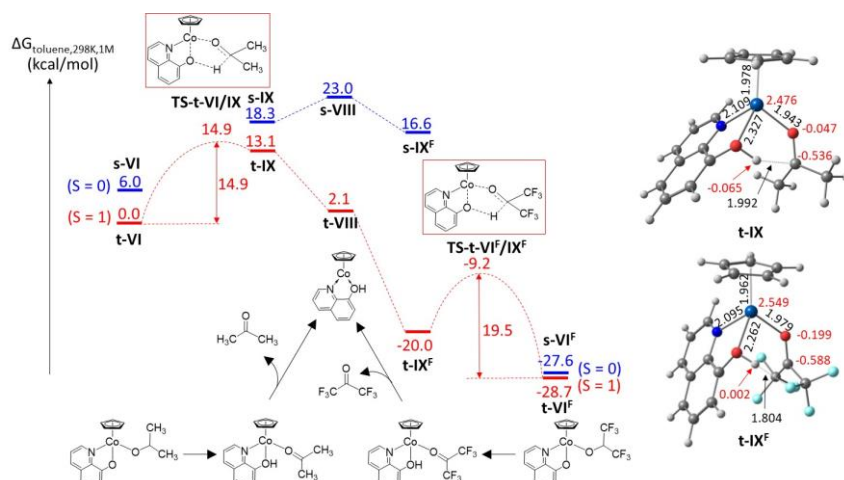


Figure 5. Comparative reductive β-H atom transfer for t-VI and t-VI^F

Left: B₃LYP-D₃-calculated free energy profile at 25°C in toluene for the reductive β-H atom transfer leading from $[\text{CpCo}(\text{Oquin})(\text{OCHR}_2)]$ (*R* = CH₃, **t-VI**; CF₃, **t-VI^F**) to **t-VIII** and R₂CO. Right: views of the optimized geometries of **t-IX** and **t-IX^F** with selected bond distances (black, in Å) and Mulliken spin densities (red).

The dramatic difference between the interaction energies of **t-VIII** with R₂CO (endoergic by 11.0 kcal mol⁻¹ for *R* = CH₃; exoergic by 22.1 kcal mol⁻¹ for *R* = CF₃) has stimulated a closer look at the electronic structures of the two “ketone adducts”. Note, in particular, how the

interaction energies of the two ketones with the singlet spin isomer (**s-VIII**) to yield the adducts **s-IX** and **s-IX^F** are, on the other, very similar, in spite of their very different nature (the acetone molecule in **s-IX** is outer sphere and H-bonded to the quinOH ligand, [CpCo(quinOH...OCMe₂)], whereas it is coordinated to the Co atom in **s-IX^F**). The spin density distributions in both compounds reveal the same features pointed out above for **t-VIII**: the Co atom has greater than two unpaired electrons while a significant spin density of opposite sign is located in the ligand system. In these cases, however, the majority of the negative spin density is distributed over the "ketone" ligand, particularly on the carbonyl C atom. All values are slightly greater for the fluorinated derivative, except for the H atom transferred to the quinOH ligand. Thus, like for **t-VIII**, the complexes are best described as having a spin quartet Co^{II} centre antiferromagnetically coupled ($S = 3/2, -1/2$) with an anion radical, which is in this case a ketyl anion radical, [Cp(quinOH)Co^{II}]⁺[OCR₂]⁻. While the electronic and spin density distributions are not dramatically different in **t-IX** and **t-IX^F**, the greater electron-withdrawing power of the two CF₃ groups may be mainly responsible for the much greater stabilization of **t-IX^F**.

Inspired by this stabilization, we explored other electron-withdrawing trapping agents that would not be able to further evolve to other products, in search for a stable adduct. Pleasingly, exposure of the brown solution derived from the **3**/NaO*t*Pr reaction in toluene to a CO atmosphere resulted in a color change from brown to orange-yellow and to the formation of a yellow-orange precipitate. An IR measurement of the supernatant solution revealed an absorption at 2040 cm⁻¹ (see SI, section S9), typical for the stretching vibration of a metal-bound CO ligand and indicating the formation of a 20-electron carbonyl adduct [Cp**Cp*(quinOH)(CO)], **5**. However, the CO binding was reversible, as the absorption was no longer observed when the product was recovered by solvent evaporation under reduced pressure. Unlike the brown solution of the presumed [Cp**Cp*(quinOH)] or ketone adduct, for which the NMR instrument could not give a stable lock and did not reveal any ¹H resonance, the product obtained after exposure to CO revealed paramagnetically shifted resonances between 45 and 25 ppm in the ¹H NMR spectrum (Figure 6 and full spectrum in the SI, section S9). The resonances shown in Figure 6 are consistent with a spin triplet ground state for compound **5**. The quinOH ligand contains 6 inequivalent aromatic protons and an additional one on the OH group. Six relatively sharp resonances are distinguishable at δ 24.5, 31.2, 34.4, 35.2, 43.3 and 43.9 ppm, but the integration of the region featuring the last two peaks is consistent with 3 protons, hinting to the presence of an underlying broader resonance, which may be due to the OH group.

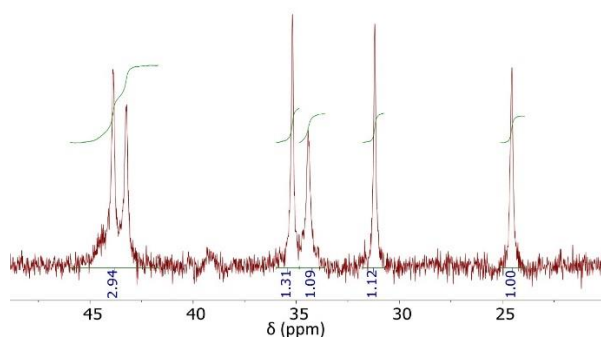


Figure 6. Characterization of compound 5

¹H NMR spectrum (in CDCl₃) of the solution obtained from the **3**/NaO*t*Pr reaction in toluene after exposure to CO.

Support for the assignment of the Figure 6 resonances to compound **5** was again provided by the DFT calculations (Figure 7). The CO addition to **t-VIII** is a rather exoergic process (by 16.7 kcal mol⁻¹), although not quite as exoergic as the addition of (CF₃)₂CO (Figure 5), and produces a spin triplet adduct, [CpCp(quinOH)(CO)] (**t-X**). This three-legged piano stool complex features two unpaired electrons quite well localized on the Co atom and only minor spin density on the ligands. The highest ligand spin density is on the CO ligand (Figure 7), whereas the quinOH ligand has the highest spin density on the N atom (+0.039). The corresponding singlet structure (**s-X**) has an optimized two-legged piano stool geometry with coplanar Co, N, CO and Cp center of gravity and a dangling OH group (Co...O = 2.886 Å)

and is located 18.2 kcal mol⁻¹ higher than the 20-electron triplet spin isomer. Relative to the [CpCo(CO)₂] compound, replacement of one CO ligand with the quinOH ligand would be essentially isoergic.

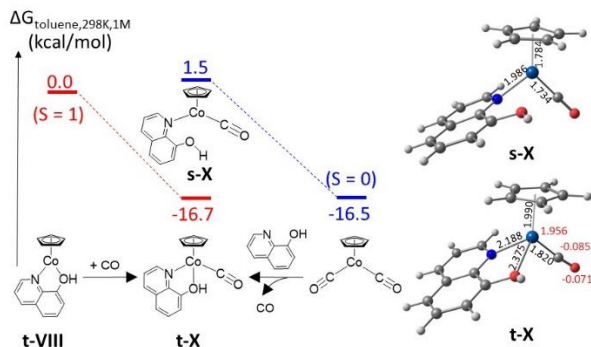


Figure 7. Relative stability of system t-X

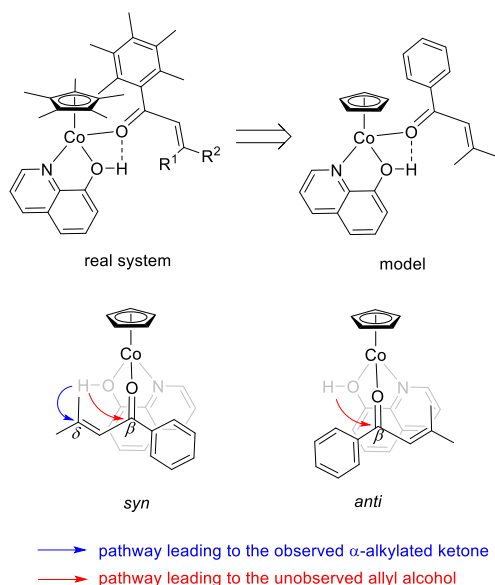
Left: B₃LYP-D₃-calculated free energy profile at 25°C in toluene for the CO addition to **t-VIII** and for the quinOH addition to [CpCo(CO)₂]. Right: views of the optimized geometries of **t-X** and **s-X** with selected bond distances (black, in Å) and Mulliken spin densities (red).

Carbon monoxide is a strong field ligand, generally leading to diamagnetic products, but spin triplet carbonyl complexes are not completely unprecedented for isolable complexes,^{38,39,41-43} although all the examples we are aware of are electronically unsaturated (< 18-electron) compounds. In this respect, the most interesting precedent is Theopold's tris(pyrazolyl)borate [Tp⁺Co(CO)] system, with 3-*i*-Pr-5-Me substituents on the Tp⁺ pyrazolyl rings. The isoelectronic half-sandwich [CpCo(CO)] complex, or ring-substituted analogues, have not been isolated under standard conditions and have only been generated by CO photodissociation from [(C₅R₅)Co(CO)₂] (R = H, Me) and isolated in low-temperature CH₄ and Ar matrices, without experimental measurement of their magnetic state.⁴⁴ Compound **5** can be described as the quinOH adduct of 16-electron [Cp^{*}Co(CO)].

(e) Selectivity of the ketone alkylation catalyzed by complex **3**

Once isopropanol is dehydrogenated to yield [Cp^{*}Co(quinOH)], the aldol cross-condensation with the bulky C₆Me₅COMe ketone produces the α,β-unsaturated ketone C₆Me₅COCH=CMe₂. As described in our previous contribution²⁸ as well in other studies,⁴⁵⁻⁴⁷ bulky ketones give the best results for this reaction because they do not yield products of aldol self-condensation. In the final step, the α,β-unsaturated ketone must be rehydrogenated. This can obviously occur by the inverse of the isopropanol dehydrogenation pathway, via coordination of the condensation product to [Cp^{*}Co(quinOH)], transfer of one proton from the quinOH ligand and two electrons from the cobalt center, and final protonation by an alcohol molecule to release the final product and regenerate the half sandwich Co^{III} alkoxide derivative [Cp^{*}Co(Oquin)(OR)], modelled by **t-VI** in the DFT study, ready to start another cycle. There is, however, a key selectivity question. Why would the coordination of the α,β-unsaturated ketone lead to selective H atom transfer to the β-C atom (δ relative to the metal center) to produce the enol tautomer of the observed ketone product, rather than to the carbonyl C atom (β relative to the metal center) to produce an unobserved allylic alcohol? This question was addressed by additional calculations.

In order to keep the calculation manageable, the C₆Me₅ aryl substituent in the ketone product was modeled by a phenyl group. As shown in Scheme 4, since both the **t-VIII** complex and the ketone are prochiral, there are two possible ketone coordination modes, yielding two diastereoisomers for the adduct **t-XI**. The *syn* mode (allyl group on the same side as the quinOH hydroxyl group) allows the H atom to be transferred to either the β or the δ C atom, whereas the allyl-*anti* mode only allows transfer to the β C atom. All three pathways were computationally explored (only in the triplet state) and the results are summarized in Figure 8.



Scheme 4. t-VIII/vinyl ketone interactions

Model system used for the calculation of the α,β -unsaturated ketone, coordination modes to [CpCo(quinOH)] and possible H transfer processes.

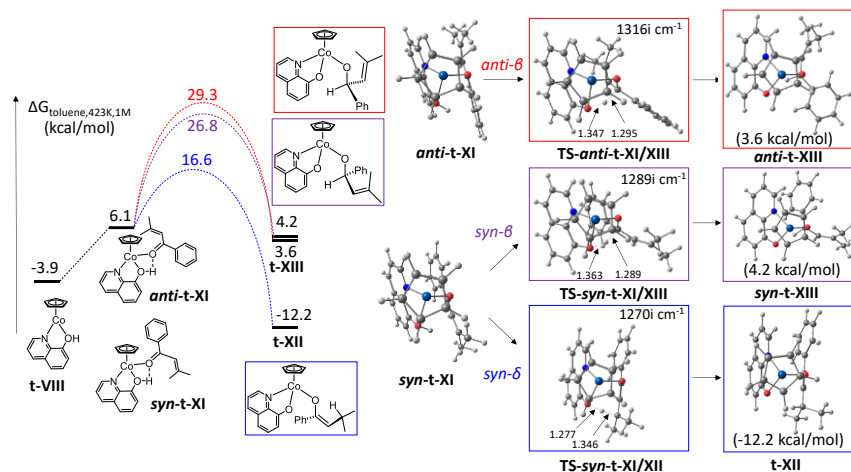


Figure 8. Conversion of t-VIII to t-XII

Left: B₃LYP-D₃-calculated free energy profile at 150°C in toluene for all possible α,β -unsaturated ketone coordination and H transfer processes. Right: optimized geometries of the [CpCo(quinOH)(PhCOCH=CMe₂)] diastereomers, transition states and H transfer products, with imaginary frequencies and O...H...C distances (in Å) for the TS structures.

The *syn*-t-XI and *anti*-t-XI isomers have the same free energy, 10.0 kcal/mol above the separated reagents. Curiously, these 20 electron triplet complexes also show significant spin density on the ketone ligand and a much more limited one on the quinOH ligand, but contrary to the t-IX and t-IX^F in Figure 5 the electronic coupling is here ferromagnetic, with spin densities of the same sign on the Co atom and on the ketone ligand (see SI, section S10). Of the three possible pathways, the single one (*syn*- δ) leading to the enolate product [CpCo(Oquin){OC(Ph)=CHCHMe₂}] (t-XII) is associated to the lowest barrier, 20.5 kcal/mol above the separate reagents and 16.6 kcal/mol from the initial alkoxide complex t-VI. The other two pathways have much greater barriers, rationalizing quite well the experimentally observed selectivity. The enolate product t-XII is more stabilized than the two isomeric allyl alkoxide diastereomers, [CpCo(Oquin){OCH(Ph)CH=CMe₂}] (*syn*- and *anti*-t-XIII). Inspection of the O...H and H...C distances shows that the *syn*- δ pathway has an earlier transition state

(shorter O...H, longer H...C) than the other two pathways, as expected on the basis of Hammond's postulate.

According to the calculated pathway, the catalyst resting state should be complex **t-VIII** and the rate-determining transition state is the reductive protonation of the α,β -unsaturated ketone intermediate. Therefore, the cycle free energy span is calculated as $\Delta G^\ddagger = 20.5 \text{ kcal mol}^{-1}$ in toluene at 150°C . The corresponding activation enthalpy is calculated as $\Delta H^\ddagger = 14.5 \text{ kcal mol}^{-1}$ ($\Delta S^\ddagger = -14.2 \text{ cal mol}^{-1} \text{ K}^{-1}$). In order to validate this calculated pathway, a kinetic investigation was thus carried out on the pentamethylacetophenone ($\text{C}_6\text{Me}_5\text{COCH}_3$) alkylation with 1-phenylethanol in toluene in the $120\text{--}150^\circ\text{C}$ range (see SI, section S11). The disappearance of the ketone substrate followed clean first order kinetics and a series of runs with different catalyst concentration confirmed a first order dependence on the cobalt complex. A rate law with first order dependence on ketone and catalyst is consistent with the calculated pathway because the energy span is the change from the resting state (catalyst **t-VIII** plus ketone product) to the limiting transition state **TS-syn-t-XI/XII**, if the aldol condensation is rapid. Finally, a variable temperature study in the $120\text{--}150^\circ\text{C}$ range followed by the Eyring analysis of the rate constant (Figure 9) provided the activation parameters as $\Delta H^\ddagger = 15.7 \pm 2.4 \text{ kcal mol}^{-1}$ and $\Delta S^\ddagger = -17.9 \pm 5.8 \text{ cal mol}^{-1} \text{ K}^{-1}$. These activation parameters are in good agreement with those calculated for the model system from **t-VIII** to **TS-syn-t-XI/XII**. In conclusion, the calculated pathway appears compatible with the experimental catalytic activity, as well as providing a rationalization for the observed selectivity.

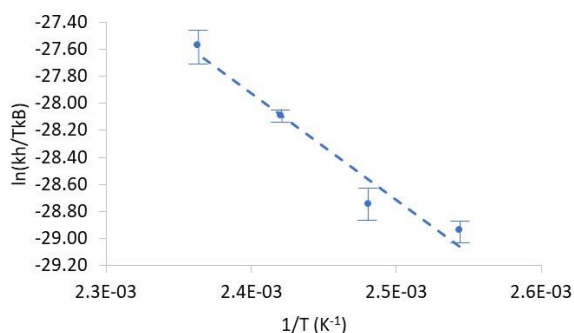


Figure 9. Experimental kinetic results for a $\text{C}_6\text{Me}_5\text{COCH}_3$ α -alkylation

Eyring analysis of the rate constants in the $120\text{--}150^\circ\text{C}$ range for the borrowing hydrogen alkylation of pentamethylacetophenone with 1-phenylethanol in toluene catalyzed by compound **3**.

(f) Alcohol dehydrogenation with the $[\text{CpCoI}_2]/\text{alkoxide}$ system

The oxindole alkylation reaction (Scheme 2, reaction 3), like the amine alkylation reaction, works best with the precatalysts **1** and **2**. However, it uses the same strong base (tBuOK) as the ketone alkylation reaction. This base is sufficiently strong to spontaneously deprotonate a secondary alcohol. Therefore, unlike for the aniline system (sections **Erreur ! Source du renvoi introuvable.** and S1), the double substitution to yield a bis(dialkoxide) CpCo^{III} derivative is now energetically accessible, see section S12. In view of the new two-proton-two-electron pathway presented in section **Erreur ! Source du renvoi introuvable.** for precatalyst **3**, it is therefore legitimate to probe a similar H transfer from the Co^{III} -coordinated alkoxide to the O atom of a second alkoxide. Both isopropoxide and 1-phenylethoxide were used as H donor in the computational model to probe this pathway, whereas the smaller methoxide was used as the proton-receiving alkoxide, again in order to limit the computational effort. Namely, the computational models for the starting point of the pathway are $[\text{CpCo}^{\text{III}}(\text{OCHMeR})(\text{OMe})]$ (**XIV**^R; R = Me, Ph). The results, shown in Figure 10, confirm that this pathway is energetically accessible. Both the starting bis(alkoxide) **XIV**^R and the final ketone-alcohol product **XV**^R are more stable in the triplet state. The free energies barriers for the triplet systems ($20.1 \text{ kcal mol}^{-1}$ for R = Ph; $22.4 \text{ kcal mol}^{-1}$ for R = Me) are greater than for the H transfer to the oxyquinolino ligand (Figure 3), but much lower than for the β -H elimination leading to the Co^{III} -H complex for the $[\text{CpCoI}_2]/\text{PhNH}_2$ system (Figure 1). The transition states **TS-t-XIV**^R/**XV**^R have imaginary frequencies of $1370i$ (R = Ph) and $1334i$ (R = Me) cm^{-1} , higher than for the Oquin system **TS-t-VI/IX**. The H...O (Ph, 1.358; Me, 1.309

Å) and H...C (Ph, 1.291; Me, 1.326 Å) distances are similar to each other, see Figure 10, like for the Oquin system. The calculated natural charges for this H atom in **TS-t-XIV^R/XV^R** are 0.269 (R = Ph) and 0.276 (R = Me), greater than those in the bis(alkoxide) precursor (**t-XIV^{Ph}**, 0.122; **t-XIV^{Me}**, 0.108) but smaller than in the ketone-alcohol product (**t-XV^{Ph}**, 0.299; **t-XV^{Me}**, 0.288). This illustrates again the increasing protic nature during the transfer. The pathway is exoergic for both systems, unlike the Oquin system where it is endoergic (Figure 3), but only because the latter produces a 20-electron compound (**t-IX**). Ketone dissociation from the **t-XV^R** H-transfer products yields the 16-electron [CpCo(MeOH)] complex, **t-XVI**, which is again more stable than the singlet spin isomer **s-XVI**.

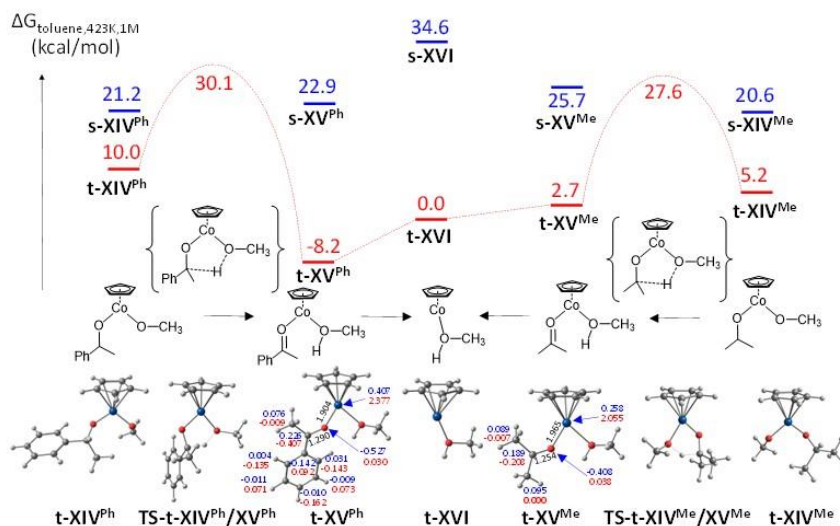


Figure 10. Conversion of t-XIV⁵ to t-XVI

Above: B₃LYP-D₃-calculated free energy profile at 150°C in toluene for the transformation of [CpCo^{II}(OCHMeR)(OMe)] to [CpCo^I(MeOH)] and RCOMe for R = Ph (left) and Me (right). Below: view of the optimized geometries with selected bond distances (black, in Å), Mulliken charges (blue) and spin densities (red) for the **t-XV^R** products. For the charges and spin densities, the hydrogen atom contributions are summed into the corresponding heavy atom figures.

The **t-XV^R** product enjoys much greater stabilization for the acetophenone system than for the acetone system: the acetone dissociation from **t-XV^{Me}** is exoergic by 2.7 kcal mol⁻¹, whereas acetophenone dissociation from **t-XV^{Ph}** is endoergic by 8.2 kcal mol⁻¹. This difference probably has the same origin as the stability difference between **t-VI^F** and **t-VI** (Figure 5). The spin density analysis shows that these “ketone” adducts are again best described as Co^{II} complexes with a ketyl radical anion (antiferromagnetic 3/2, -1/2 system), with a more accentuated spin distribution in the acetophenone complex **t-XV^{Ph}** (2.377 for Co and a total spin density of -0.589 on the ketone ligand, of which the majority is on the carbonyl C atom), see Figure 10. Complex **t-XV^{Me}** has the two unpaired electrons essentially localized on the Co center (2.055) and a much smaller spin density of opposite sign on the acetone ligand.

(g) Reductive protonation of the 3-alkylidene-2-oxindole.

After oxidative deprotonation of R(Me)CHOH to RCOMe, as described in the previous section, and after C-C bond formation with the deprotonated oxindole, as shown in Scheme 2,²⁹ the 3-alkylidene-2-oxindole intermediate can coordinate to **t-XVI** and be reductively protonated by the Co^I-coordinated alcohol molecule, producing a 3-alkyl-2-hydroxyindole, which finally tautomerizes to the final 3-alkyl-2-oxindole. Unlike the reductive protonation of the α,β-unsaturated ketone by the Oquin system described in section **Erreur ! Source du renvoi introuvable.** (Scheme 4 and Figure 8), the metal complex is not prochiral in the present case, therefore coordination of the unsaturated intermediate can only lead to one stereoisomer. For the model system, coordination of the oxindole condensation product, leading to the adduct **t-XVII**, is only slightly endoergic by +2.8 kcal mol⁻¹ at 150°C (though exoergic by -2.6 kcal mol⁻¹ at 25°C). This adduct, like the acetophenone adduct **t-XVPh**

(Figure 10) reveals the contribution of an antiferromagnetic Co^{II} -(alkoxy radical) structure, as suggested by the Mulliken spin density analysis, see Figure 11. The electron delocalization in the 3-alkylidene-2-oxindole ligand places the majority of the ligand spin density on the δ -C atom (-0.627).

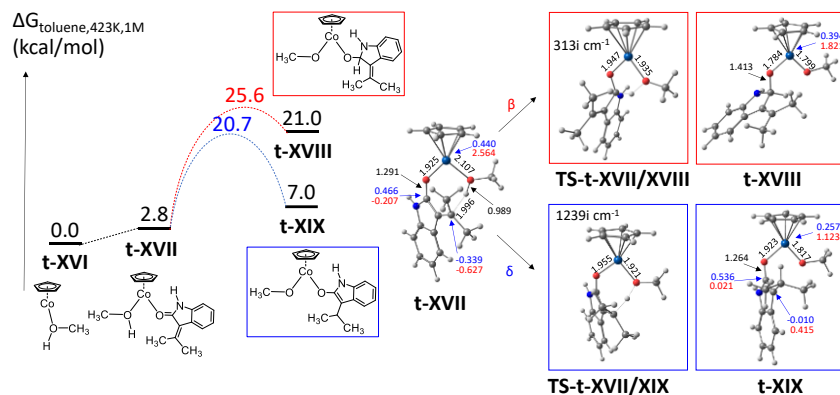


Figure 11. Conversion of t-XVI to t-XIX

Left: B₃LYP-D₃-calculated free energy profile at 150°C in toluene for the 3-isopropylidene-2-oxindole coordination to and intramolecular reductive protonation by [CpCo(MeOH)] (**t-XV**). Right: views of the optimized geometries with selected bond distances (black, in Å), Mulliken charges (blue) and spin densities (red).

Once again, the proton can be delivered either to the β - or to the δ -C atom but only the latter occurs. The greater aptitude for transfer to the δ -C atom is already suggested by the ground state structure of **t-XVII**, shown in Figure 11. The O-H bond is oriented toward the δ -C atom with a relatively short H...C $^{\delta}$ contact of 1.996 Å, which is related to the charge distribution in the molecule. The Mulliken charge analysis reveals a negative charge on this carbon atom (-0.339) and a positive one on the carbonyl C $^{\beta}$ atom in the indole ring (+0.466). For comparison, the Mulliken charge of the C $^{\gamma}$ atom in the indole ring is -0.097 and those of the C $^{\epsilon}$ atoms of the two methyl groups are +0.068 and +0.107, with the charges of the H atoms summed into the heavy atoms. Proton transfer to the C $^{\beta}$ atom leads to loss of electron delocalization in the indole 5-membered ring and is therefore thermodynamically less favorable, yielding a 3-isopropylidene-indoline-2-oxyl cobalt product **t-XVIII** at a relatively high energy (21.0 kcal mol⁻¹ relative to **t-XVI**) via **TS-t-XVII/XVIII**, with a barrier of 22.8 kcal mol⁻¹ relative to **t-XVII** or 25.6 kcal mol⁻¹ relative to **t-XVI**. On the other hand, transfer of the MeOH proton to the C $^{\delta}$ atom, leading to the *ipr*-substituted oxindolate derivative **t-XIX**, proceeds through **TS-t-XVII/XIX** with a barrier of 20.7 kcal mol⁻¹ from the unsaturated intermediate **t-XVI** and yields a more stable 3-isopropyl-indole-3-oxy product at 7.0 kcal mol⁻¹ from **t-XVI**. Note that the electronic and bond distance parameters of **t-XVIII** agree with its description as a spin triplet Co^{III} bis(alkoxide): the spin density is almost fully localized on the Co atom, the oxindole C-O bond has lengthened from 1.291 to 1.413 Å, while the Co-O(oxindole) distance has shortened and the Co-O(MeOH) distance has lengthened along the H transfer reaction to become essentially equivalent. On the other hand, the more stable product **t-XIX** has a lower spin density on the Co atom, the C-O and Co-O(oxindole) distances have not significantly changed, and part of the spin density has been transferred to the oxindole ligand, mostly on the C $^{\gamma}$ atom (0.415). This suggests the contribution of a ferromagnetic Co^{II}-(oxindole radical) (+1/2, +1/2) configuration to the electronic structure.

(h) Alcohol dehydrogenation by reductive deprotonation for [CpCo]₂/PhNH₂

Once realized that the alcohol can be dehydrogenated by β -H atom abstraction as a proton by an internal base, coupled to electron delivery to the metal (intramolecular oxidative deprotonation) according to Scheme 1(c₁), it is natural to conceive the same process with intervention of an external base, e.g. aniline, according to Scheme 1(c₂). As shown in section **Erreur! Source du renvoi introuvable.** (Figure 1), alcohol deprotonation and iodide exchange, yielding triplet [CpCo(OCHMePh)] (**t-I**) is accessible at kinetically competent rates. Abstraction of the alkoxide β -H atom by aniline, though a van der Waals adduct **t-I**...H₂NPh, leads to the triplet ketone adduct [CpCo(O=CMePh)]PhNH₃⁺ (**t-XX**), which is

placed by the DFT calculation at only +6.8 kcal mol⁻¹ from **t-I**, namely at 17.9 kcal mol⁻¹ from triplet [CpCoI₂], see Figure 12. This salt is characterized by short contacts between one ammonium proton and both the O (2.400 Å) and the carbonyl C (2.463 Å) atom of the ketone ligand, as well as by contact between a second ammonium proton and both the I ligand (2.405 Å) and the O atom (2.621 Å). By analogy with the ketone complexes **t-XVPh** (Figure 10) and **t-XVII** (Figure 11), the spin density is delocalized on the ketone ligand, suggesting the contribution of an antiferromagnetic Co^{II}-(alkoxyl radical) configuration. The transition state for the β-H transfer to aniline (**TS-t-I/XX**) is placed at 15.5 kcal mol⁻¹ from **t-I** + PhNH₂, or 26.6 kcal mol⁻¹ from triplet [CpCoI₂]. Therefore, the intermolecular oxidative deprotonation of isopropanol for the [CpCoI₂]/PhNH₂ system via [CpCo(O/Pr)]/PhNH₂ occurs at competitive rates relative to the intramolecular process for the [CpCo(Oquin)I] catalyst via [CpCo(Oquin)(O/Pr)] (Figure 3) and to the intramolecular process for the [CpCoI₂]/alkoxide catalyst via [CpCo(OMe)(O/Pr)] (Figure 10).

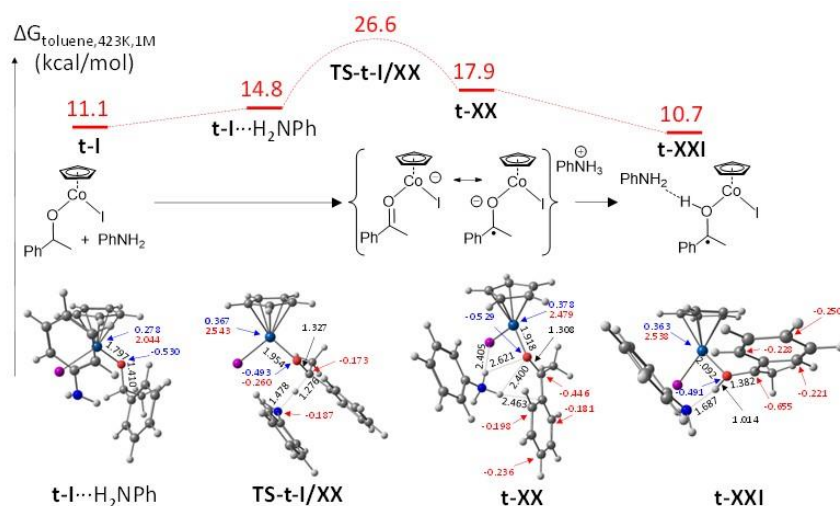


Figure 12. Oxidative alkoxide deprotonation by external base

Above: B₃LYP-D₃-calculated free energy profile at 150°C in toluene for the intermolecular oxidative deprotonation of [CpCo^{III}(O/Pr)] (**t-I**) by aniline. Below: view of the optimized geometries with selected bond distances (black, in Å), Mulliken charges (blue) and spin densities (red).

The PES exploration leading to the location of **TS-t-I/XX** also revealed the existence of another isomer at lower energy, corresponding to a [CpCo(PhMeCOH...NH₂Ph)] complex (**t-XXI**) where the proton has been transferred to the O atom of the ketone ligand, see Figure 12. Further exploration of the PES indicated that a direct 1,2 H shift from **t-I**...NH₂Ph to generate **t-XXI** is not viable, hence the isomerization requires transit through **t-XX**. The **TS-t-XX/XXI** could not be located. The spin density distribution in **t-XXI** is similar to that in **t-XX**, with an even greater positive value on the Co atom and greater negative values on the ketone atoms, suggesting that the antiferromagnetic Co^{II}-radical formulation may be more appropriate. It is also interesting to note that the Mulliken charge on the Co atom is similar in **t-XX** and **t-XXI** and greater than in the Co^{III} precursor **t-I**. On the other hand, the O atom maintains a similar negative charge in the three systems. The final imine hydrogenation step of the catalytic cycle, after ketone condensation with the aniline and water elimination, can occur by the reverse imine coordination and reductive protonation, where a proton and two electrons are delivered by the ammonium cation and cobalt center, respectively, followed by amine release by exchange with an alcohol molecule. These steps have not been modelled by DFT calculations.

CONCLUSION

The results of our computational investigations on three different but mechanistically related Cp*Co^{III}/base-catalyzed hydrogen borrowing processes, notably the triplet ground state of the key intermediates [CpCoI₂], [CpCo(OCHR¹R²)] and [CpCo(Oquin)(OCHMe₂)], have unveiled the incongruence of the observed absolute and relative activities of the various

catalytic systems with the established dogmas in transfer hydrogenation chemistry (Scheme 1 (a) and (b)). Further DFT explorations have led to the discovery of a new paradigm in transfer hydrogenation for the oxidative activation of alcohols, according to which the catalytic system in a higher oxidation state metal center acts as an electron repository and allows the alkoxide β -H atom to be removed as a proton, either intramolecularly by a ligand, e.g. Oquin for the $[\text{Cp}^*\text{Co}(\text{Oquin})]/\text{KOtBu}$ system or an alkoxide for the $[\text{Cp}^*\text{Co}_2]/\text{KOtBu}$ system, and even intermolecularly by an external base, e.g. aniline for the $[\text{Cp}^*\text{Co}_2]/\text{aniline}$ system.

The experimental validation of this new mechanistic scenario (Scheme 1 (c)) was complicated by the paramagnetism of most of the involved intermediates. In particular, the key $[\text{Cp}^*\text{Co}(\text{quinOH})]$ species, a relatively rare example of a spin triplet 18-electron organometallic species, which is indicated by the DFT study to play the role of resting state in the $[\text{Cp}^*\text{Co}(\text{Oquin})]/\text{KOtBu}$ -catalyzed aryl ketone α -alkylation, yields NMR silent spectra. However, CO addition to solutions of this compound leads to the spectroscopic identification (IR, paramagnetic ^1H NMR) of the $[\text{Cp}^*\text{Co}(\text{Oquin})(\text{CO})]$ adduct, an unusual 20-electron spin triplet carbonyl complex. Although all steps in the investigated catalytic cycles involve two-electron changes (no radical reactivity), electronic redistribution occurs in many key intermediates with involvement of non-innocent ligands, yielding electronic configurations that can better be described as featuring a Co^{I} ion with either a 1/2 or 3/2 spin state ferro- or antiferromagnetically coupled with a ligand anion radical.

The results of this study are alerting us to a possible broader involvement of this oxidative alkoxide activation pathway in transfer hydrogenation or borrowing hydrogen catalysis when employing redox-active and relatively high oxidation state catalysts and strong bases. Many already described catalytic systems probably deserve to be scrutinized again under this light.

EXPERIMENTAL PROCEDURES

See the supplemental information for the experimental investigations of the stoichiometric 3/base/alcohol reactions (section S8), of the $[\text{Cp}^*\text{Co}(\text{Oquin})(\text{OH})]$ trapping reaction (section S9) and of the catalyzed $\text{C}_6\text{Me}_5\text{COCH}_2/\text{PhCH}(\text{CH}_3)\text{OH}$ reaction kinetics (section S11), and for the computational details (section S13).

Resource availability

Lead contact

Further information and requests for resources should be directed to and will be fulfilled by the lead contact, Rinaldo Poli (Rinaldo.poli@lcc-toulouse.fr).

Materials availability

This study did not generate new materials.

Data and code availability

The datasets generated during this study are available at <https://hal.archives-ouvertes.fr/hal-03244195>.

SUPPLEMENTAL INFORMATION

A single document, available as pdf file, contains:

Section S1. DFT results of the iodide-alkoxide exchange in the $[\text{CpCo}_2]/\text{PhNH}_2$ system

Section S2. DFT relaxed scans leading to the location of the triplet TS for the 2-phenylethanol β -H elimination on spin triplet $[\text{CpCo}(\text{OCHMePh})]$

Section S3. DFT calculations of the energy associated to the I/O/Pr exchange process in $\text{CpCo}(\text{Oquin})$

Section S4. Comparison between the DFT-optimized geometry of **s-V** and the X-ray diffraction geometry of $[\text{Cp}^*\text{Co}(\text{Oquin})]$

Section S5. DFT exploration of the β -H elimination in $[\text{CpCo}(\text{Oquin})(\text{OCHMe}_2)]$ (**VI**)

Section S6. DFT relaxed scans for the β -H transfer from a zwitterionic intermediate

Section S7. DFT relaxed scans for the β -H transfer from the OCHMe_2 ligand in $[\text{CpCo}(\text{Oquin})(\text{OCHMe}_2)]$ to the Oquin O atom

Section S8. Experimental details and DFT computations on the decomposition of [Cp*Co(Oquin)(OCHR²R³)]
Section S9. Trapping reaction of [Cp*Co(quinOH)]
Section S10. Spin densities on compounds *anti*- and *syn-t-XI*
Section S11. Experimental details and results of the kinetics study
Section S12. DFT results of the iodide-alkoxide exchange in the [CpCoI₂]/tBuOK system
Section S13. Computational details
Section S14. Energy data, Cartesian coordinates and <S²> for all optimized systems

ACKNOWLEDGMENTS

We gratefully acknowledge the financial support provided by CEFIPRA (grant number IF-5805-1). This work was granted access to the resources of the CICT (Centre Interuniversitaire de Calcul de Toulouse, project CALMIP).

AUTHOR CONTRIBUTIONS

PC: investigation (experimental); BS: conceptualization, supervision, writing (review and editing), project administration, funding acquisition; EM: supervision, writing (review and editing); RP: conceptualization, formal analysis, investigation (computational), data curation, writing (original draft), project administration, funding acquisition.

DECLARATION OF INTERESTS

The authors declare no competing interests.

REFERENCES*

1. Brown, J.M., ed. (1999). Hydrogenation of Functionalized Carbon-Carbon Double Bonds (Springer-Verlag).
2. Blaser, H.U., Malan, C., Pugin, B., Spindler, F., Steiner, H., and Studer, M. (2003). Selective hydrogenation for fine chemicals: Recent trends and new developments. *Adv. Synth. Catal.* **345**, 103-151.
3. Chen, B., Dingerdissen, U., Krauter, J.G.E., Rotgerink, H., Mobus, K., Ostgard, D.J., Panster, P., Riermeier, T.H., Seebald, S., Tacke, T., and Trauthwein, H. (2005). New developments in hydrogenation catalysis particularly in synthesis of fine and intermediate chemicals. *Appl. Catal. A* **280**, 17-46. [10.1016/j.apcata.2004.08.025](https://doi.org/10.1016/j.apcata.2004.08.025).
4. Palmer, A.M., and Zanotti-Gerosa, A. (2010). Homogenous asymmetric hydrogenation: Recent trends and industrial applications. *Current Opinion in Drug Discovery & Development* **13**, 698-716.
5. Fleury-Bregeot, N., de la Fuente, V., Castillon, S., and Claver, C. (2010). Highlights of Transition Metal-Catalyzed Asymmetric Hydrogenation of Imines. *ChemCatChem* **2**, 1346-1371. [10.1002/cctc.201000078](https://doi.org/10.1002/cctc.201000078).
6. Stefane, B., and Pozgan, F. (2016). Metal-Catalysed Transfer Hydrogenation of Ketones. *Topics in Current Chemistry* **374**, 18. [10.1007/s41061-016-0015-5](https://doi.org/10.1007/s41061-016-0015-5).
7. Dub, P.A., and Gordon, J.C. (2017). Metal Ligand Bifunctional Catalysis: The "Accepted" Mechanism, the Issue of Concertedness, and the Function of the Ligand in Catalytic Cycles Involving Hydrogen Atoms. *ACS Catal.* **7**, 6635-6655. [10.1021/acscatal.7b01791](https://doi.org/10.1021/acscatal.7b01791).
8. Seo, C.S.G., and Morris, R.H. (2019). Catalytic Homogeneous Asymmetric Hydrogenation: Successes and Opportunities. *Organometallics* **38**, 47-65. [10.1021/acs.organomet.8b00774](https://doi.org/10.1021/acs.organomet.8b00774).
9. Dobereiner, G.E., and Crabtree, R.H. (2010). Dehydrogenation as a Substrate-Activating Strategy in Homogeneous Transition-Metal Catalysis. *Chem. Rev.* **110**, 681-703. [10.1021/cr900202j](https://doi.org/10.1021/cr900202j).
10. Gunanathan, C., and Milstein, D. (2013). Applications of Acceptorless Dehydrogenation and Related Transformations in Chemical Synthesis. *Science* **341**, 1229712/1229711-1229711, 1229712. [10.1126/science.1229712](https://doi.org/10.1126/science.1229712).
11. Corma, A., Navas, J., and Sabater, M.J. (2018). Advances in One-Pot Synthesis through Borrowing Hydrogen Catalysis. *Chem. Rev.* **118**, 1410-1459. [10.1021/acs.chemrev.7b00340](https://doi.org/10.1021/acs.chemrev.7b00340).
12. Kalck, P., and Urrutigoity, M. (2018). Tandem Hydroaminomethylation Reaction to Synthesize Amines from Alkenes. *Chem. Rev.* **118**, 3833-3861. [10.1021/acs.chemrev.7b00667](https://doi.org/10.1021/acs.chemrev.7b00667).
13. Bailey, B.C., Schrock, R.R., Kundu, S., Goldman, A.S., Huang, Z., and Brookhart, M. (2009). Evaluation of Molybdenum and Tungsten Metathesis Catalysts for Homogeneous Tandem Alkane Metathesis. *Organometallics* **28**, 355-360. [10.1021/om800877q](https://doi.org/10.1021/om800877q).
14. Doerksen, R.S., Meyer, C.C., and Krische, M.J. (2019). Feedstock Reagents in Metal-Catalyzed Carbonyl Reductive Coupling: Minimizing Preactivation for Efficiency in Target-Oriented Synthesis. *Angew. Chem. Int. Ed.* **58**, 14055-14064. [10.1002/anie.201905532](https://doi.org/10.1002/anie.201905532).

15. Bullock, R.M. (2004). Catalytic ionic Hydrogenations. *Chem. Eur. J.* **10**, 2366-2374.
16. Chirik, P.J. (2015). Iron- and Cobalt-Catalyzed Alkene Hydrogenation: Catalysis with Both Redox-Active and Strong Field Ligands. *Acc. Chem. Res.* **48**, 1687-1695. [10.1021/acs.accounts.5b00134](https://doi.org/10.1021/acs.accounts.5b00134).
17. Dub, P.A., Henson, N.J., Martin, R.L., and Gordon, J.C. (2014). Unravelling the Mechanism of the Asymmetric Hydrogenation of Acetophenone by [RuX₂(diphosphine)(1,2-diamine)] Catalysts. *J. Am. Chem. Soc.* **136**, 3505-3521. [10.1021/ja411374j](https://doi.org/10.1021/ja411374j).
18. Hayes, J.M., Deydier, E., Ujaque, G., Lledós, A., Malacea-Kabbara, R., Manoury, E., Vincendeau, S., and Poli, R. (2015). Ketone Hydrogenation with Iridium Complexes with "non N-H" Ligands: The Key Role of the Strong Base. *ACS Catal.* **5**, 4368-4376.
19. Sandoval, C.A., Ohkuma, T., Muniz, K., and Noyori, R. (2003). Mechanism of asymmetric hydrogenation of ketones catalyzed by BINAP/1,2-diamine-ruthenium(II) complexes. *J. Am. Chem. Soc.* **125**, 13490-13503. [10.1021/ja030272c](https://doi.org/10.1021/ja030272c).
20. Abdur-Rashid, K., Clapham, S.E., Hadzovic, A., Harvey, J.N., Lough, A.J., and Morris, R.H. (2002). Mechanism of the Hydrogenation of Ketones Catalyzed by trans-Dihydro(diamine)ruthenium(II) Complexes. *J. Am. Chem. Soc.* **124**, 15104-15118.
21. Badiei, Y.M., Wang, W.H., Hull, J.F., Szalda, D.J., Muckerman, J.T., Himeda, Y., and Fujita, E. (2013). Cp*Co(III) Catalysts with Proton-Responsive Ligands for Carbon Dioxide Hydrogenation in Aqueous Media. *Inorg. Chem.* **52**, 12576-12586. [10.1021/ic401707u](https://doi.org/10.1021/ic401707u).
22. Roy, S., Sharma, B., Pecaut, J., Simon, P., Fontecave, M., Tran, P.D., Derat, E., and Artero, V. (2017). Molecular Cobalt Complexes with Pendant Amines for Selective Electrocatalytic Reduction of Carbon Dioxide to Formic Acid. *J. Am. Chem. Soc.* **139**, 3685-3696. [10.1021/jacs.6b11474](https://doi.org/10.1021/jacs.6b11474).
23. Kumar Pandey, I., Kumar, A., and Choudhury, J. (2020). Electrocatalytic CO₂ Reduction with a Half-Sandwich Cobalt Catalyst: Selectivity towards CO. *Chem. Asian J.* **15**, 904-909. [10.1002/asia.201901805](https://doi.org/10.1002/asia.201901805).
24. Dahiya, P., Gangwar, M.K., and Sundararaju, B. (2021). Well-defined Cp*Co(III)-catalyzed Hydrogenation of Carbonates and Polycarbonates. *ChemCatChem* **13**, 934-939. [10.1002/cctc.202001490](https://doi.org/10.1002/cctc.202001490).
25. Pagano, J.K., Stelmach, J.P.W., and Waterman, R. (2015). Cobalt-catalyzed ammonia borane dehydrocoupling and transfer hydrogenation under aerobic conditions. *Dalton Trans.* **44**, 12074-12077. [10.1039/c5dt00108k](https://doi.org/10.1039/c5dt00108k).
26. Gangwar, M.K., Dahiya, P., Emayavaramban, B., and Sundararaju, B. (2018). Cp*Co-III-Catalyzed Efficient Dehydrogenation of Secondary Alcohols. *Chem. Asian J.* **13**, 2445-2448. [10.1002/asia.201800697](https://doi.org/10.1002/asia.201800697).
27. Emayavaramban, B., Chakraborty, P., Manoury, E., Poli, R., and Sundararaju, B. (2019). Cp*Co(III)-Catalyzed Direct Amination of Secondary Alcohols. *Organic Chemistry Frontiers* **6**, 852-857.
28. Chakraborty, P., Gangwar, M.K., Emayavaramban, B., Manoury, E., Poli, R., and Sundararaju, B. (2019). Well-defined Cp*Co(III)-Catalyzed α -Alkylation of Ketones with Secondary Alcohols. *ChemSusChem* **12**, 3463-3467. [10.1002/cssc.201900990](https://doi.org/10.1002/cssc.201900990).
29. Chakraborty, P., Garg, N., Manoury, E., Poli, R., and Sundararaju, B. (2020). C-Alkylation of Various Carbonucleophiles with Secondary Alcohols Under Co^{III}-Catalysis. *ACS Catal.* **10**, 8023-8031. [10.1021/acscatal.0c01728](https://doi.org/10.1021/acscatal.0c01728).
30. Huffman, J.W. (1983). Metal-ammonia reductions of cyclic aliphatic ketones. *Acc. Chem. Res.* **16**, 399-405. [10.1021/ar00095a002](https://doi.org/10.1021/ar00095a002).
31. Zimmerman, H.E. (2012). A Mechanistic Analysis of the Birch Reduction. *Acc. Chem. Res.* **45**, 164-170. [10.1021/ar2000698](https://doi.org/10.1021/ar2000698).
32. Poli, R. (1996). Open-Shell Organometallics as a Bridge Between Werner-Type and Low-Valent Organometallic Complexes. The Effect of the Spin State on the Stability, Reactivity and Structure. *Chem. Rev.* **96**, 2135-2204.
33. Hamon, P., Toupet, L., Hamon, J.-R., and Lapinte, C. (1994). Synthesis, X-ray crystal structure and magnetic properties of the six-coordinated intermediate-spin iron(II) complex [Fe(h⁵-C₅Me₅)(h²-Ph₂PCH₂CH₂PPh₂)(s-O=CMe₂)]⁺CF₃SO₃⁻. *J. Chem. Soc., Chem. Commun.*, 931-932.
34. Sinopalnikova, I.S., Peganova, T.A., Belkova, N.V., Deydier, E., Daran, J.-C., Shubina, E.S., Kalsin, A.M., and Poli, R. (2018). Ruthenium p-cymene iminophosphonamide complexes: activation under basic conditions and transfer hydrogenation catalysis. *Eur. J. Inorg. Chem.*, 2285-2299
35. Reiher, M. (2002). Theoretical study of the Fe(phen)₂(NCS)₂ spin-crossover complex with reparametrized density functionals. *Inorg. Chem.* **41**, 6928-6935.
36. Morin, A.N., Detrembleur, C., Jérôme, C., Tullio, P.D., Poli, R., and Debuigne, A. (2013). Effect of head-to-head addition in vinyl acetate reversible deactivation radical polymerization: why is Co(acac)₂-mediated polymerization so much better? *Macromolecules* **46**, 4303-4312. [10.1021/ma400651a](https://doi.org/10.1021/ma400651a).
37. Kim, D., Rahaman, S.M.W., Mercado, B.O., Poli, R., and Holland, P.L. (2019). The Roles of Iron Complexes in Catalytic Radical Alkene Cross-Coupling. *J. Am. Chem. Soc.* **141**, 7473-7485. [10.1021/jacs.9b02117](https://doi.org/10.1021/jacs.9b02117).

38. Detrich, J.L., Reinaud, O.M., Rheingold, A.L., and Theopold, K.H. (1995). Can spin state change slow organometallic reactions? *J. Am. Chem. Soc.* *117*, 11745-11748. 10.1021/ja00152a015.
39. Reinaud, O.M., and Theopold, K.H. (1994). Hydrogen tunneling in the activation of dioxygen by a tris(pyrazolyl)borate cobalt complex. *J. Am. Chem. Soc.* *116*, 6979-6980. 10.1021/ja00094a080.
40. Zhang, C., Zhang, G., Luo, S., Wang, C., and Li, H. (2018). Base-catalyzed selective esterification of alcohols with unactivated esters. *Org. Biomol. Chem.* *16*, 8467-8471. 10.1039/c8ob02411a.
41. Calderazzo, F., Marchetti, F., Poli, R., Vitali, D., and Zanazzi, P.F. (1982). Synthesis and Crystal and Molecular Structure of Mixed-valence Tetranuclear and Trinuclear Compounds of Rhenium Obtained by Di-iodine Oxidation of Rhenium(I) Carbonyl Complexes. *J. Chem. Soc., Dalton Trans.*, 1665-1670.
42. Philipp, C.C., Young, C.G., White, P.S., and Templeton, J.L. (1993). Dicarboxyltungsten(II) thiolate complexes of hydrotris(3,5-dimethylpyrazolyl)borate. *Inorg. Chem.* *32*, 5437-5443.
43. Saleh, A.A., Pleune, B., Fettingner, J.C., and Poli, R. (1997). Hydrotris(pyrazolyl)borate Molybdenum Chemistry: Spin Triplet Sixteen-electron Carbonyl Derivatives of Molybdenum(II), and the X-ray Structure of the Oxo Compound $\{HB(3,5-Me_2C_3N_2H)_3\}MoO_2$. *Polyhedron* *16*, 1391-1397.
44. Rest, A.J., Whitwell, I., Graham, W.A.G., Hoyano, J.K., and McMaster, A.D. (1987). Photoactivation of Methane by h^5 -Cyclopentadienyl and Substituted h^5 -Cyclopentadienyl Group 8 Metal Dicarboxyl Complexes. $[M(h^5-C_5R_5)(CO)_2]$ ($M = Rh$ or Ir , $R = H$, or Me), and Dicarboxyl(h^5 -indenyl)iridium: A Matrix Isolation Study. *J. Chem. Soc., Dalton Trans.*, 1181-1190.
45. Akhtar, W.M., Cheong, C.B., Frost, J.R., Christensen, K.E., Stevenson, N.G., and Donohoe, T.J. (2017). Hydrogen Borrowing Catalysis with Secondary Alcohols: A New Route for the Generation of beta-Branched Carbonyl Compounds. *J. Am. Chem. Soc.* *139*, 2577-2580. 10.1021/jacs.6b12840.
46. Akhtar, W.M., Armstrong, R.J., Frost, J.R., Stevenson, N.G., and Donohoe, T.J. (2018). Stereoselective Synthesis of Cyclohexanes via an Iridium Catalyzed (5+1) Annulation Strategy. *J. Am. Chem. Soc.* *140*, 11916-11920. 10.1021/jacs.8b07776.
47. Thiyagarajan, S., and Gunanathan, C. (2019). Catalytic Cross-Coupling of Secondary Alcohols. *J. Am. Chem. Soc.* *141*, 3822-3827. 10.1021/jacs.9b00025.